SELECTIVE LIMITING BY A MOVING LEAST SQUARES TECHNIQUE

Xesús Nogueira[*], Ignasi Colominas[*], Luis Cueto-Felgueroso[†], Héctor Gómez[*], Fermín Navarrina[*], Manuel Casteleiro[*]

[*]Group of Numerical Methods in Engineering (GMNI)
Department of Applied mathematics, Civil Engineering School,
Universidade da Coruña, Campus de Elviña, 15071, A Coruña, Spain
e-mail: xnogueira@udc.es, web page: http://caminos.udc.es/gmni/index.html

[†]Department of Civil and Environmental Engineering,
Massachusetts Institute of Technology, Cambridge, MA 02139, USA

Key words: Shock-capturing, Compressible flows, High-order methods, Unstructured grids.

s it is known, the use of high-order numerical methods for the resolution of compressible flows on unstructured grids is a very complex problem. While ENO and WENO [1, 2] schemes obtain very good results when structured grids are used, their application to unstructured grids is complicated due to the difficulties for choosing the appropriate stencil. On the other hand, the most usual approach in this kind of grids is to use methods based on a Taylor reconstruction of the variables with slope limiters [3]. However, most of the existing slope limiters are only designed for second-order schemes, by limiting the first derivative of the Taylor reconstruction. Unfortunately, the straightforward application of slope limiters to higher-order schemes by limiting the higher-order derivatives, may result in bad behavior of the solution. Moreover, slope limiters usually identify regions near smooth extrema as requiring limiting. As a result, the optimal higher-order convergence rate is reduced. A possible way of improving this behavior is to develop a selective limiting method, by measuring the smoothness of the solution and switching off the limiter when the solution is not sharp enough. With this procedure, optimal higher-order convergence rate in smooth areas can be recovered. In this work we present the a new MLS-based sensor to detect shock waves on general grids, used with standard slope-limiters. We show the results of several benchmarks, in one and two dimensions. The results are very promising, comparable to those of essentially non-oscillatory (ENO) and weighted ENO (WENO) schemes on structured grids.

1 Introduction

High-order finite volume methods usually work with a Taylor reconstruction of the variables inside each control volume I:

$$\boldsymbol{U}(\boldsymbol{x}) = \boldsymbol{U}_I + \boldsymbol{\nabla U}_I \cdot (\boldsymbol{x} - \boldsymbol{x}_I) + ... \tag{1}$$

However, it is known that the numerical schemes built in that way are not monotonic. Thus, new extrema will appear when the high-order scheme is applied to non-smooth flows. In order to force monotonicity, a very common technique is the use of slope-limiters. Slope-limiters are usually designed for second order approximations, and they limit the reconstruction as:

$$\boldsymbol{U}(\boldsymbol{x}) = \boldsymbol{U}_I + \chi_I \boldsymbol{\nabla U}_I \cdot (\boldsymbol{x} - \boldsymbol{x}_I) \tag{2}$$

where χ is a value between 0 and 1 that is computed with any slope limiter algorithm. However, it is known that this approach could result in a more diffusive and less accurate solution, due to the fact that the slope limiter may be active even in regions where the flow is not-smooth. The application of a selective limiting procedure can alleviate this problem and to recover optimal higher-order convergence rate in smooth areas. A selective limiting procedure requires a sensor to decide where the limitation is applied.

A sensor can be designed based on the multiresolution properties of the Moving Least Squares approximations [4]. The MLS method tries to approximate the value of a function in terms of MLS shape functions (N). These shape functions are built from a discrete set of points (nodes) so that a MLS approximation of a vector variable $\boldsymbol{U}_I$ in the control volume I can be written as:

$$\boldsymbol{U}_I(\boldsymbol{x}) = \sum_{j=1}^{n_I} \boldsymbol{U}_j N_j(\boldsymbol{x}) \tag{3}$$

where n_I is the number of neighbors of I.

In the construction procedure of the MLS shape functions, kernel functions are required to weight the value of the different points of the neighborhood of I [5]. In this work we have used the following 1D exponential kernel to build the MLS shape functions:

$$W(x, x^*, \kappa_x) = \frac{e^{-\left(\frac{s}{c}\right)^2} - e^{-\left(\frac{dm}{c}\right)^2}}{1 - e^{-\left(\frac{dm}{c}\right)^2}} \tag{4}$$

with $s = |x_j - x^*|$, $d_m = max\left(|x_j - x^*|\right)$, with $j = 1, \ldots, n_{x^*}$, $c = \frac{d_m}{2\kappa_x}$, x^* is the reference point (the point where the MLS-shape functions are evaluated), and n_{x^*} is the number of neighbors of the reference point. Moreover x is the position of every cell centroid of the stencil and κ_x is a shape parameter. A tipical value for this parameter is $\kappa = 1$ (see [6]). A 2D kernel is obtained by multiplying two 1D kernels. Thus, the 2D exponential kernel is the following:

$$W_j(\boldsymbol{x}, \boldsymbol{x}^*, \kappa_x, \kappa_y) = W_j(x, x^*, \kappa_x) W_j(y, y^*, \kappa_y) \tag{5}$$

2

A MLS approximation can be seen as a low-pass filtering. This is the basis of the MLS sensor presented in this work. Thus, in the next section we will introduce briefly the MLS-based filters, and then we will apply this results to the development of the MLS sensor.

2   MLS-based Filters

The development of explicit numerical filters has attracted the attention of researchers of the field of turbulence, particularly in the case of Large-Eddy simulation (LES). LES methodology needs a separation between the different scales of the flow, and this separation may be performed with explicit numerical filters. The use of the *Reproducing Kernel Particle Method* (RKPM)) as a filter for turbulence problems was proposed in [8]. Thus, a MLS approximation of a variable can be seen as a low-pass filtering of the variable. Following equation (3) we write for a given variable Φ:

$$\overline{\Phi_I} = \sum_{j=1}^{n_I} N_j(\boldsymbol{x})\Phi_j \tag{6}$$

where n is the number of neighbors of the *stencil* of cell I, and we use the notation $^-$ to indicate a filtered variable.

The filter properties are analyzed by the study of its transfer function, that is, a mathematical model that indicates the answer of a system for a certain input. In this case, the input is the nodal value of the variable. The answer is the result of applying a MLS approximation to the nodal values of the variable. Then, the transfer function associated to equation (6) is:

$$\hat{G}(\kappa) = \sum_{j=1}^{n_I} N_j(\boldsymbol{x})e^{i\kappa(x_j-x_I)} \tag{7}$$

$\hat{G}(\kappa)$ is determined by the number of points of the stencil, the kind of basis and the kernel function used to build the MLS shape functions.

In figure 1 we plot the transfer function of MLS filters with kernel (4) for different values of the κ parameter. In that figure, a value of $\hat{G} = 1$ indicates no filtering. We note that we can vary the properties of the MLS-based filter by modifying the shape parameter κ. This is the basis of the proposed MLS-based sensor.

3   A MLS-based sensor

The connection between MLS approximations and wavelets has been successfully used for error estimation and adaptivity [9]. This connection makes possible to define a wavelet function from MLS shape functions, as we will show next. With the kernel given by equation (4), the approximation of the solution given by (3) keeps all the resolutions and properties of the solution $\mathbf{U}(\mathbf{x})$, until the κ scale. On a wavelet framework, MLS shape
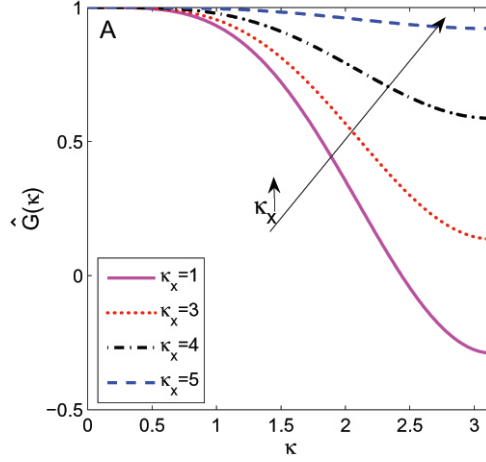
Figure 1: 1D transfer function of MLS approximations with the exponential kernel

functions could be seen as scale functions and κ as the scale parameter. Different values of κ lead to different resolutions. Then, a wavelet function can be obtained by defining two sets of MLS shape functions, with different shape parameters of the kernel function, and so, keeping different resolutions. Thus, we obtain the $\kappa_H - scale$ and $\kappa_L - scale$ approximations,

$$\mathbf{U}^{\kappa_H}(\mathbf{x}) = \sum_{j=1}^{n_I} \mathbf{U}_j N_j^{\kappa_H}(\mathbf{x}), \qquad \mathbf{U}^{\kappa_L}(\mathbf{x}) = \sum_{j=1}^{n_I} \mathbf{U}_j N_j^{\kappa_L}(\mathbf{x}) \tag{8}$$

where the $\kappa_H - scale$ approximation corresponds with the high-resolution approximation, and the $\kappa_L - scale$ corresponds with the low-resolution approximation.

So, the wavelet function $\mathbf{\Phi}$ can be written as:

$$\mathbf{\Phi}(\mathbf{x}) = \mathbf{N}^{\kappa_H}(\mathbf{x}) - \mathbf{N}^{\kappa_L}(\mathbf{x}) \tag{9}$$

On the other hand, the $\kappa_H - scale$ solution can be written as the sum of the low scale contribution ($\mathbf{U}^{\kappa_L}(\mathbf{x})$) and the high scale part ($\mathbf{\Psi}(\mathbf{x})$).

$$\mathbf{U}^{\kappa_H}(\mathbf{x}) = \mathbf{U}^{\kappa_L}(\mathbf{x}) + \mathbf{\Psi}(\mathbf{x}) \tag{10}$$

being

$$\mathbf{\Psi}(\mathbf{x}) = \sum_{j=1}^{n_I} \mathbf{U}_j \mathbf{\Phi}_j(\mathbf{x}) = \sum_{j=1}^{n_I} \mathbf{U}_j (\mathbf{N}^{\kappa_H}(\mathbf{x}) - \mathbf{N}^{\kappa_L}(\mathbf{x})) \tag{11}$$

This decomposition process could continue for the low scale part $\mathbf{U}^{\kappa_L}(\mathbf{x})$ and so on.

The function $\mathbf{\Psi}(\mathbf{x})$ is a measure of the smoothness of $\mathbf{U}(\mathbf{x})$. We propose to use it as a sensor in a selective limiting procedure. Thus, when $\mathbf{\Psi}(\mathbf{x})$ is greater than a given value,

the limiter is switched on at that point, but it remains switched off ($\chi = 1$) at the points that are smaller than the threshold value.

On the other hand, to completely define the methodology, we have to define the threshold value. We consider the density as the reference variable and we use it to define the threshold value T_v as:

$$T_v = C_{lc} \left| \nabla \rho \right|_I (A_I)^{\frac{1}{d}} / M \tag{12}$$

A_I is the size (area in 2D) of the control volume I, d is the number of dimensions of the problem, C_{lc} is a parameter, and M is the free stream Mach number. If $C_{lc} = 0$, there is no selective limiting, and the usual slope-limiter algorithm is used in the whole domain of computation. We have included a Mach number scaling in order to reduce the variability of the C_{lc} parameter, but in general it is problem dependent. In our experience, a good initial guess is $C_{lc} = 0.32$. Note that it is also possible to use a local Mach number instead the free-stream Mach number for the scaling.

Thus, the slope limiter is switched on when:

$$\Psi_\rho = \sum_{j=1}^{n_I} \rho_j (N_j{}^{\kappa_H}(\mathbf{x}) - N_j{}^{\kappa_L}) > T_v \tag{13}$$

In order to improve the robustness of the selective limiting in unstructured grids, a good practice is to switch on the limiter in all the points of the stencil of the control volume I when the limiter is switched on in I. If more dissipation is required to avoid wiggles, we could reduce the value of the C_{lc} parameter. This methodology fits very well with the use of the FVMLS method [5], a higher-order finite volume method based on MLS approximations of the derivatives. We have used this method in our calculations, although the MLS sensor can be used with any other numerical technology. In all the examples presented here, we have computed the $\kappa_H - scale$ shape function with $\kappa_x = \kappa_y = 6$ and the $\kappa_L - scale$ shape function with $\kappa_x = \kappa_y = 1$.

4 Numerical examples

4.1 A first 1D test. Toro's problem

Next we present a 1D-test designed to check the accuracy and robustness of numerical methods for hyperbolic equations: 1D Euler equations are solved with the following initial conditions: $(\rho, v, p) = (1.0, 0.0, 1000)$ if $x < 0.5$ and $(\rho, v, p) = (1, 0, 0.01)$ if $x \geq 0.5$. This setup of the problem is the same as the proposed in [10]. It is the left half of the blast wave problem of Woodward and Colella [11]. The computational domain is $[-5, 5]$, and 100 cells are used. With this example we want to show the effect of a variation in the parameter C_{lc}, so no Mach scaling has been used. Exact solutions have been computed with the NUMERICA library [12].
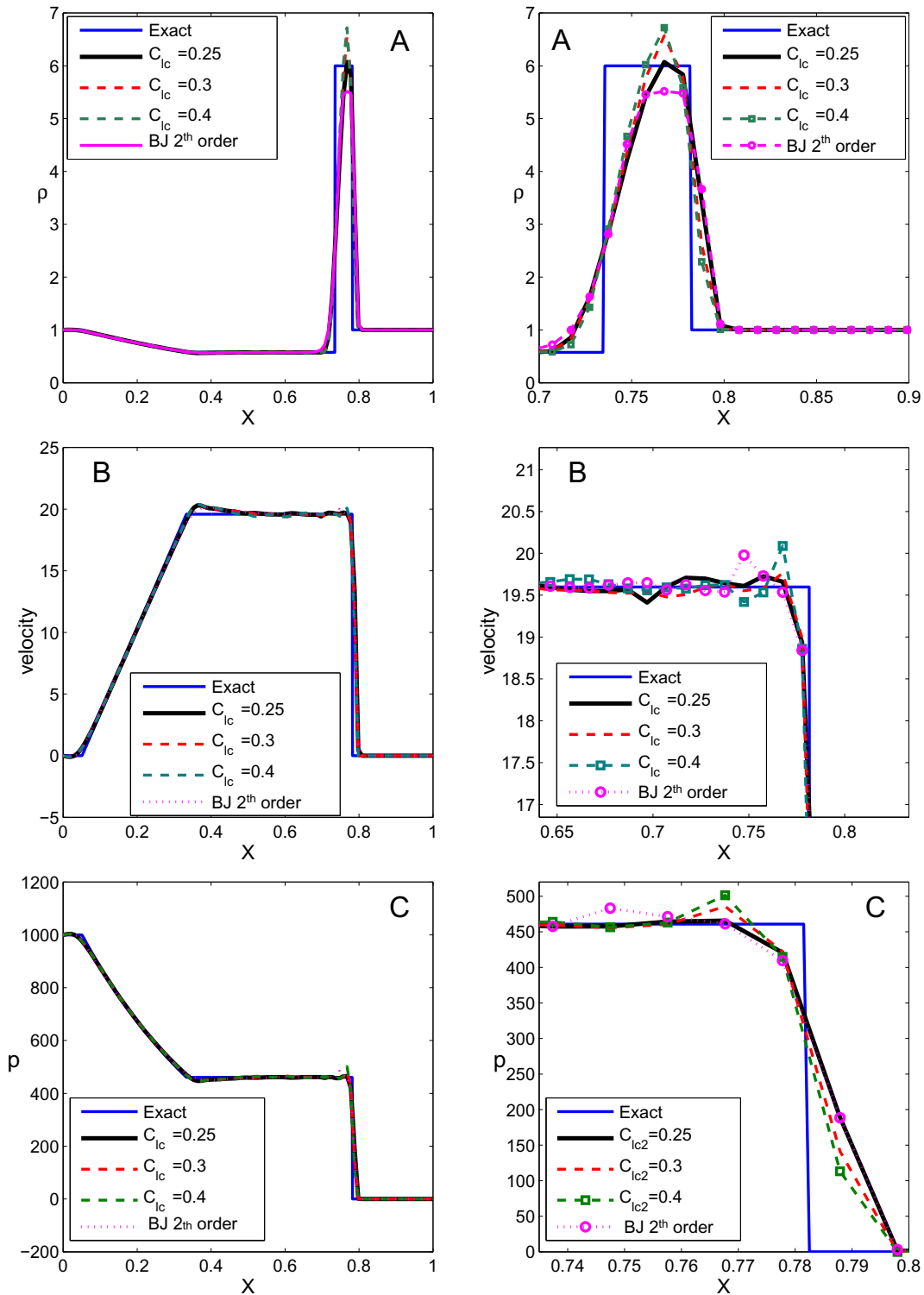
Figure 2: Toro's problem [10], 100 cells, results for $t = 0.012$. (A) density,(B) velocity (C) pressure, for different values of C_{lc} parameter and comparison with the results for a second-order FV-MLS scheme with slope-limiter. On the right we plot a detail of the shock zones. No local Mach number was used for the scaling.

4.2 2D examples. Shu-Osher problem

We show the results for the 2D extension of the Shu-Osher problem [13]. The 2D Euler equations are solved in $[-5, 5] \times [-1, 1]$, with initial conditions $(\rho, v_x, v_y, p) = (3.857, 2.629, 0, 10.333)$ if $x < -4$, and $(\rho, v_x, v_y, p) = (1 + 0.2\sin(5x), 0, 0, 1)$ if $x \geq -4$. We use a structured 400×80 cartesian grid. Figure 3 (left) shows the density and the function Ψ_ρ after 1.8 seconds, while on the right it is shown a cut in $y = 0$ of the function Ψ_ρ for this case. It is clearly seen that it indicates the points where the solution is not smooth.
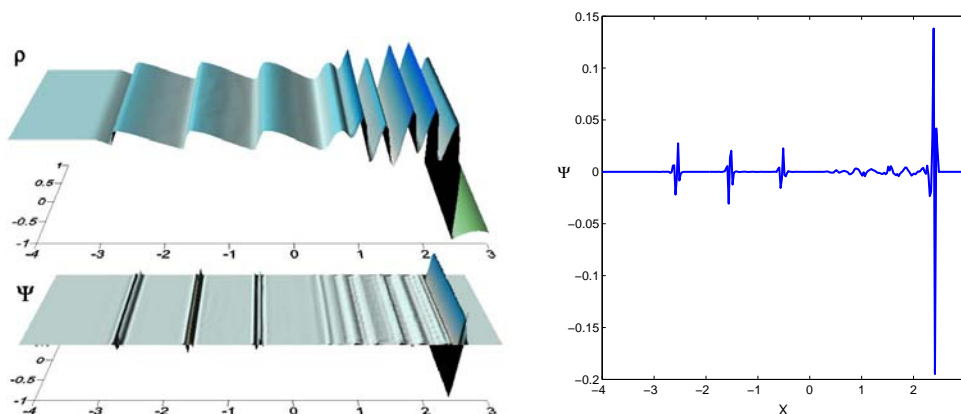

Figure 3: Third-order solution of the density (ρ) to the Shu-Osher problem and function Ψ_ρ for the Shu-Osher problem (left). On the right hand side, a cross section at $y = 0$ shows more clearly the appearance of Ψ_ρ, and how this function detects the points where the reference variable (density) is not smooth.

4.3 2D examples. Transonic flow

As an example of application for 2D unstructured grids, we show a classical transonic example: the subsonic flow past a NACA 0012 airfoil, with Mach number $M = 0.8$ and angle of attack $\alpha = 1.25$. The grid used is made of quadrilaterals and we have placed 64 control volumes along each side of the profile. The total number of elements is 5322. The external boundary of this grid is a circumference. The radius of this circumference is 25 chords of the profile. We have used a fourth order FV-MLS scheme with the MLS sensor and the limiter designed by Barth and Jespersen [14] (BJ), but any other limiter could be used with our approach. The value of the shape parameters of the kernel are $\kappa_x = \kappa_y = 1$ for the spatial approximation. In figure 4 (top left) we show the Mach contours and the cells where the BJ limiter is switched on (shaded). In this cells we apply the selected slope limiting algorithm as usual. The figure also show (top right) the cells where the BJ coefficient is limiting ($\chi \neq 1$).With the selective limiting, fourth order reconstruction is recovered at wall-boundary cells upstream and downstream of the main shock, since the limiter is switched off. This effect is shown in figure 5, where we plot the

entropy generation on the profile surface. We note the effective reduction of the entropy generation when the MLS-based selective limiting is used. This reduction is bigger in the smoother part of the flow, upstream of the strong shock. Selective limiting also eliminates the spurious effect of negative entropy generation when the same χ is used to limit the first, second and third derivatives of the Taylor reconstruction in a fourth order scheme. This effect does not appear with the use of the second order FV-MLS scheme and BJ limiter.
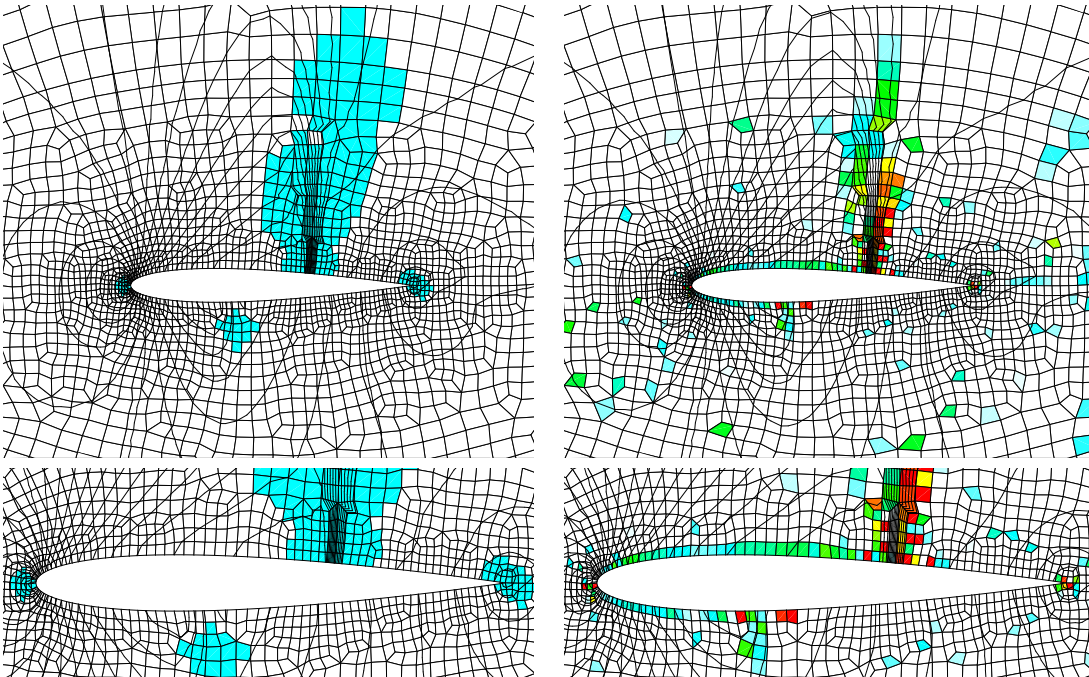

Figure 4: Limited cells and Mach contours for the transonic flow past a NACA 0012 airfoil, with Mach number $M = 0.8$ and angle of attack $\alpha = 1.25$. In the left, shaded cells indicate the cells in which the limiter is switched on. In the right, colored cells indicate the cells where the BJ coefficient is limiting ($\chi \neq 1$). In the bottom, we show a zoom of the profile, where is clearly seen that the selective limiting recovers the higher-order scheme, since the limiter is switched off in the boundary cells upstream and downstream of the shock, while the BJ limiter coefficient is limiting.

Drag and lift coefficients are shown in table 1. It is shown that the results with selective limiting are closer to the AGARD reference data [15] than the results obtained when the BJ limiter is used without selective limiting. The reduction in the drag coefficient indicates the less dissipative character of the fourth order scheme with selective limiting. We note that the fourth order BJ scheme without selective limiting is more dissipative than the second order one. This effect is also related with the use of the same χ to limit all the derivatives. Finally, in figure 6 we show a plot of the pressure coefficient (C_p) for the different schemes, and we compare it with a reference solution obtained on a finer grid of 12243 control volumes, with 128 cells placed along each side of the profile.
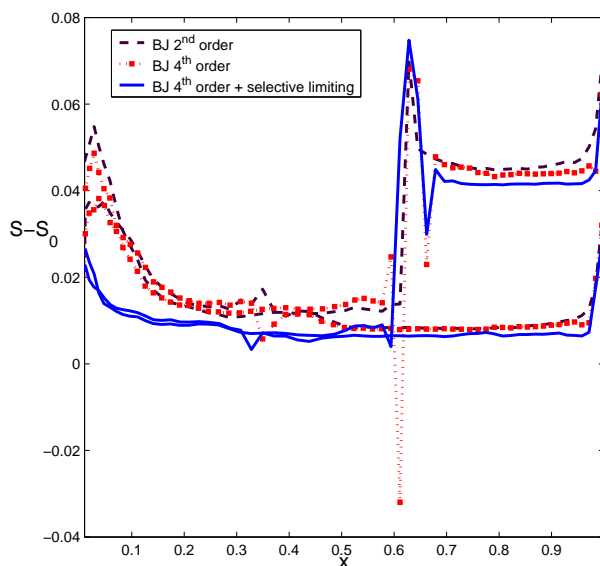
Figure 5: Entropy generation over the profile surface. S_0 is the free stream entropy. Selective limiting reduces the entropy generation, and this effect is bigger upstream of the shock. The use of a fourth order scheme with BJ limiter does not reduce the generation of entropy, and it presents the problem of negative entropy generation. This anomalous behavior is due to the use of the same value of χ to limit all the derivatives. This problem is also alleviated with selective limiting.

Conclusion

A multidimensional shock detection technique based on the Moving Least Squares method that can be used in both structured and unstructured grids has been presented. Multiscale properties of MLS are used to separate the high scale components of the solution to built a MLS-based wavelet function of a reference variable. When the wavelet function is bigger than a threshold, the slope limiter is switched on. The method is robust and it allows to keep the maximum order of accuracy of the scheme in smooth regions. Nowadays the authors are working on several aspects that are in a preliminary stage, as the establishment of the value of the C_{lc} parameter and to analyze the influence of the shape parameter κ on the properties of the proposed method.

Table 1: Lift (C_L) and drag (C_D) coefficients

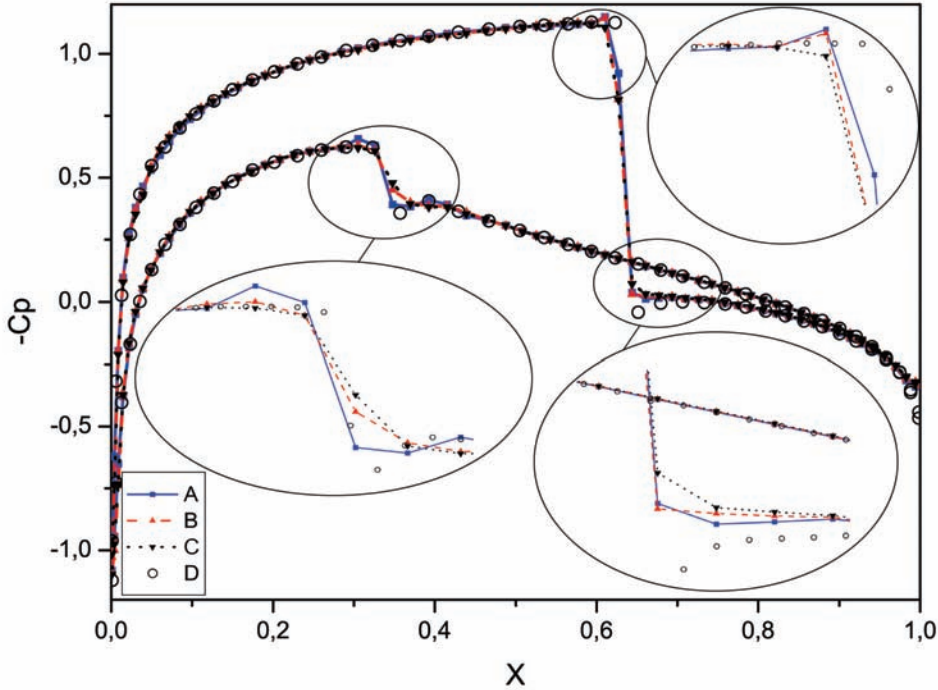| Scheme	C_L	C_D
BJ 2nd order	0.341	2.465E-02
BJ 4th order	0.342	2.486E-02
BJ 4th order + MLS sensor	0.343	2.317E-02
AGARD reference [15] (structured 192×39)	0.347	2.221E-02

Figure 6: Pressure coefficient for different schemes and zoom of the shock zones. A- Fourth order MLS-based selective limiting. B- Fourth order BJ scheme. C- Second order BJ scheme. D- Reference solution obtained with a second order BJ scheme on a finer grid. Some points of the reference solution have been skipped for clarity in the non-zoomed picture.

References

REFERENCES

[1] Harten, A., Engquist, B., Osher, S., Chakravarthy, S., Uniformly high order essentially nonoscillatory schemes, III, *Journal of Computational Physics*, Vol. 71, pp. 231-303, 1987.

[2] Shu, C.-W., *Essentially non-oscillatory and weighted essentially non-oscillatory schemes for hyperbolic conservation laws*, ICASE Report 97-65, 1997.

[3] Barth, T. J., Frederickson, P. O., Higher-order solution of the Euler equations on unstructured grids using quadratic reconstruction, AIAA paper 90-0013, 1990.

[4] Lancaster, P., Salkauskas, K., Surfaces generated by moving least squares methods, *Mathematics of Computation*, Vol 37 (155), pp. 141158, 1981.

[5] Cueto-Felgueroso, L., Colominas, I., Nogueira, X., Navarrina, F., Casteleiro, M., Finite volume solvers and Moving Least-Squares approximations for the compressible Navier-Stokes equations on unstructured grids,*Computer Methods in Applied Mechanics and Engineering*, Vol. 196, pp. 4712-4736, 2007.

[6] Nogueira, X., Cueto-Felgueroso, L., Colominas, I., Khelladi, S.,On the simulation of wave propagation with a higher-order finite volume scheme based on Reproducing Kernel Methods, *Computer Methods in Applied Mechanics and Engineering*, doi: 10.1016/j.cma.2009.12.015.

[7] Sjögreen, B., Yee, H. C., Multiresolution Wavelet Based Adaptive Numerical Dissipation Control for High Order Methods, *Journal of Scientific Computing*, Vol. 20, pp. 211-255, 2004.

[8] Wagner, G. J. and Liu, W. K., Turbulence simulation and multiple scale subgrid models, *Computational Mechanics*, **25**, 117-136, 2000.

[9] Liu, W. K, Hao, W., Chen, Y., Jun, S., Gosz, J., Multiresolution Reproducing Kernel Particle Methods, *Computational Mechanics*, Vol. 20, pp. 295-309, 1997.

[10] Toro, E. F., *Riemann Solvers and Numerical Methods for Fluid Dynamics*. A Practical Introduction, Second edition, Berlin: Springer Verlag, 1999.

[11] Woodward, P., Colella, P., The Numerical Simulation of Two-Dimensional Fluid Flow with Strong Shocks, *Journal of Computational Physics*, **54**, 115-173, 1984.

[12] Toro, E. F., *NUMERICA, a Library of Source Codes for Teaching, Research and Applications*, http://www.numeritek.com/, Numeritek Limited, UK, 1999.

[13] Shu, C.-W., Osher, S., Efficient implementation of essentially non-oscillatory shock-capturing schemes II, *Journal of Computational Physics*, Vol. 83, pp. 32-78, 1989.

[14] Barth, T. J., Jespersen, D. C., The design and application of upwind schemes on unstructured meshes, AIAA-89-0366, 1989.

[15] AGARD Fluid Dynamics Panel. Test Cases for Inviscid Flow Field Methods, AGARD Advisory Report AR-211,AGARD, May 1985